

The enigma of Neoproterozoic giant ooids—Fingerprints of extreme climate?

Elizabeth J. Trower¹

¹Department of Geological Sciences, University of Colorado Boulder, Boulder, CO, USA 80309.

Corresponding author: Elizabeth J. Trower (lizzy.trower@colorado.edu)

Key Points:

- Giant ooids are a rare carbonate facies that occur in strata underlying a number of Neoproterozoic glacial deposits.
- Giant ooid diameter was applied to constrain Neoproterozoic seawater carbonate saturation state, temperature, and alkalinity.
- Neoproterozoic giant ooids indicate hot or cold, but not moderate, climate at low latitudes preceding the onset of glaciations.

Abstract

Geologists have documented at least fourteen occurrences of “giant ooids”, a geologically rare type of carbonate allochem, in Neoproterozoic successions at low paleo-latitudes. Recent experiments and modeling demonstrated that ooid size reflects an equilibrium between precipitation and abrasion rates, such that ooid size could be used as a geological proxy for CaCO_3 mineral saturation state (Ω). Here, the documented sizes of Neoproterozoic giant ooids were applied to estimate seawater Ω , which provided a novel approach to constraining temperature, partial pressure of CO_2 , and alkalinity preceding Neoproterozoic glaciations. The results suggest that giant ooid formation was most plausible with seawater alkalinity elevated over its present value by at least a factor of two, and either much warmer (40°C) or much colder (0°C) climate than modern tropical carbonate platforms, which have important and divergent implications for climate states and ecosystem responses prior to the initiation of each Neoproterozoic glaciation.

Plain Language Summary

Ooids are a type of calcium carbonate sediment grain composed of a set of concentric layers formed around a small particle. Although most ooids are sand-size grains (<2 mm in diameter), rare cases, referred to as “giant ooids”, are much larger, with some >1 cm in diameter. Geologists have suggested that these giant ooids reflected unusual seawater chemistry, but the exact conditions required for their formation remained unknown. Although giant ooids are geologically rare, a surprising number of occurrences have been described from Neoproterozoic rocks (1000–541 million years old) that underlie sedimentary layers deposited by low paleo-latitude glaciations (i.e., “Snowball Earth” events). This study used the grain diameters of Neoproterozoic ooids to estimate the temperature and composition of seawater when they formed. The results showed that Neoproterozoic seawater must have either been very hot or very cold just prior to these glaciations, a finding that challenges either climate models of this era or conceptual models of common modes of carbonate sediment formation and deposition.

1 Introduction

Neoproterozoic carbonate successions are host to enigmatic and geologically rare carbonate allochems known as “giant ooids”, uncommonly large concentrically-coated carbonate

grains (>2 mm in diameter). Sumner and Grotzinger (1993) noted that giant ooids occur more commonly and were generally larger in diameter during Neoproterozoic time than any other period in Earth history; additional observations have confirmed this occurrence pattern (cf. Table 3 in Thorie et al., 2018). Geologists have speculated that the formation of giant ooids required exceptionally high calcium carbonate mineral saturation state and higher current velocities than are characteristic of modern ooid shoals (Sumner & Grotzinger, 1993; Swett & Knoll, 1989). Yet, this hypothesis has remained untested and does not clearly explain why giant ooids are not more common in older Precambrian successions.

Giant ooids have been documented in Neoproterozoic strata in Greenland, Svalbard, Canada, Alaska (USA), California (USA), Siberia, Mongolia, India, and Australia (Batten et al., 2004; Day et al., 2004; Fromhold & Wallace, 2011; Gutstadt, 1968; Macdonald, et al., 2009a, 2009b; Petrov, 2018; Singh, 1987; Srivastava, 2006; Sumner & Grotzinger, 1993; Swett & Knoll, 1989; Teitz & Mountjoy, 1989; Thorie et al., 2018; Trower & Grotzinger, 2010; Zenger, 1976). Grotzinger and James (2000) noted that many of these giant ooids closely underlie glacial diamictites and/or cap carbonates (Table 1) associated with prolonged glacial episodes that occurred during the Cryogenian period (the “Sturtian” and the “Marinoan” glaciations), known as “Snowball Earths” because geological evidence indicates widespread glaciation extending to low latitudes (Chumakov, 2007; Evans, 2000; Hoffman et al., 1998, 2017; Kirschvink, 1992; Trindade & Macouin, 2007). Some giant ooid occurrences are directly overlain by glacial strata, while others are separated by ~100-300 m of stratigraphy (in one case, ~1 km) (Table 1). The durations of time elapsed between deposition of giant ooids and glacially-associated sediments are not well-constrained geochronologically (cf. Table 4 in Thorie et al., 2018). There is also evidence of a third glacial episode during the Ediacaran period (the “Gaskiers”), although it appears unlikely that it constituted a Snowball Earth due to the paucity of low-latitude glacial deposits (Hoffman & Li, 2009); it is not clear that the four cases of giant ooids documented in Ediacaran strata precede the Gaskiers glaciation (Table 1). These stratigraphic associations of Neoproterozoic giant ooids suggest that a better understanding of the environmental conditions required for giant ooid formation would provide new constraints for models of the global carbon cycle and climate during this dynamic era.

Recent experiment and modeling demonstrated that ooid size reflects an equilibrium between precipitation and abrasion rates (Trower et al., 2017), with the implication that ooid size

in the rock record can be used to infer the calcium carbonate mineral saturation state of ancient seawater, Ω , where $\Omega = \frac{[Ca^{2+}][CO_3^{2-}]}{K_{sp}}$ (K_{sp} is the solubility product constant). These reconstructed Ω values can then be applied to estimate the other parameters that describe the carbonate system: the partial pressure of CO_2 (pCO_2), alkalinity (ALK), pH, and the concentration of dissolved inorganic carbon (DIC). Here, this approach is applied to Neoproterozoic giant ooids to provide a novel constraint on Neoproterozoic pCO_2 , alkalinity, and temperature prior to the initiations of the Cryogenian Snowball Earths and during the Ediacaran Period.

2 Methods

Based on the giant ooid occurrences documented by Sumner and Grotzinger (1993), with the addition of occurrences described more recently (Batten et al., 2004; Day et al., 2004; Fromhold & Wallace, 2011; Macdonald, et al., 2009a, 2009b; Petrov, 2018; Srivastava, 2006; Thorie et al., 2018; Trower & Grotzinger, 2010), Neoproterozoic giant ooids range from 2 to 25 mm in diameter (D) (Table 1). Within this range, $D = 5$ mm and $D = 10$ mm were chosen as representative grain sizes for which to assess characteristic Ω values—the former representative of a grain diameter observed in the majority of the giant ooid deposits and the latter a conservative representative of the largest ooids in these deposits (Table 1). Many of these giant ooid occurrences have been described as having been originally composed of aragonite (Hood and Wallace, 2018), but additional $CaCO_3$ minerals were also explored for this analysis.

An equilibrium ooid size is the grain diameter, D_{eq} , at which the precipitation rate $R_{precipitation}$ and the abrasion rate $R_{abrasion}$ are equal (Trower et al., 2017). Abrasion rate can be estimated from the rock record by measuring D and determining a characteristic bed shear velocity, u_* (Trower et al., 2017). There are several potential approaches to estimating u_* : the simplest is to leverage the observation from modern systems that ooids are typically transported near the threshold of suspension and estimate u_* by assuming Rouse number $P = 2.5$, where $P = \frac{w_s}{\kappa u_*}$; $\kappa = 0.41$ is the von Kármán constant and w_s is settling velocity calculated following Dietrich (1982) with grain diameter (D), sediment density (ρ_s), fluid density (ρ_f), and fluid kinematic viscosity (ν). Alternatively, if bedforms are preserved in the rock record, their dimensions can be used to estimate u_* (Lapotre et al., 2017; Southard & Boguchwal, 1990).

Because bedform dimensions are not well-documented for Neoproterozoic giant ooid occurrences, $P = 2.5$ was used to estimate a range for u_* corresponding to the range of giant ooid sizes (Figure S1). Consistent with this choice, most giant ooids have high sphericities, suggesting that they dominantly experienced collisional abrasion during saltation, rather than frictional abrasion during rolling and sliding (Sipos et al., 2018). $R_{abrasion}$ can then be calculated following Lamb et al. (2008) and Trower et al. (2017):

$$R_{abrasion} = \frac{\pi A_I \rho_s Y w_i^3 D^3}{6 k_v \sigma_T^2 H_{fall}} \quad (1)$$

where σ_T is tensile strength and Y is Young's modulus of elasticity (1 MPa and 20 GPa, respectively, following Trower et al., 2017); w_i is impact velocity normal to the bed, calculated following Lamb et al. (2008); H_{fall} is the typical height particles are transported above the bed, calculated following Lamb et al. (2008); $k_v = 9 \times 10^5$ is a non-dimensional constant calibrated for ooid abrasion by Trower et al. (2017); and $A_I \approx 1/3$ (Sklar and Dietrich, 2004) accounts for the fact that the time between particle-bed impacts depends on the time for a particle to be transported from the bed up to H_{fall} , in addition to the time to settle back to the bed. H_{fall} and w_i both depend on water depth, H . $H = 5$ m was chosen as a representative water depth; sensitivity tests indicate that varying water depth has a negligible effect on the resulting Ω prediction (Figure S2). Application of this abrasion model relies on the assumptions (1) that ooid diminution primarily occurs through abrasion of mud-size ($<62.5 \mu\text{m}$) carbonate particles rather than fragmentation of larger particles, which is consistent with experimental observations of abrasion of carbonate sand (Trower et al., 2019) and limestone pebbles (Attal and Lavé, 2009), and (2) that abrasion rates calibrated for sand-size carbonate particles (Trower et al., 2017) can be extrapolated to pebble-size carbonate particles, which is supported by similarity in modeled rates with experimental rates for limestone pebbles (Attal and Lavé, 2009) (Figure S3).

For each combination of (D, u_*) , one can estimate the precipitation rate required to sustain that D as the equilibrium ooid size: $R_{precipitation} = f \cdot R_{abrasion}$, where $f = (0, 1]$ is intermittency of movement. For the purposes of this analysis, $f = 0.01$ (i.e., sediment is actively transported 1% of the time) was chosen as a lower bound on this parameter—resulting $R_{precipitation}$ estimates are therefore minimum values (Figure S4). This intermittency value is somewhat less than observed in modern ooid shoals— $f = 0.1$ - 0.25 on Ambergris shoal in the Turks and Caicos

Islands (Trower et al., 2018)—but this infrequent active transport could be explained by the large heights and wavelengths characteristic of gravel bedforms (Carling, 1999). The value of Ω required for each D_{eq} can be solved for by rearranging the volumetric precipitation rate equation for the carbonate mineral of interest:

$$R_{precipitation} = k(\Omega - 1)^n \cdot \frac{M}{\rho_s} \cdot A_{surface} \quad (2)$$

where k is the rate constant ($\mu\text{mol}/\text{m}^2/\text{hr}$), n is the reaction order (dimensionless), M is the molar mass of the calcium carbonate mineral (g/mol), and $A_{surface}$ is the ooid surface area (m^2).

Four scenarios with different mineralogy and/or temperature were simulated, using estimates for seawater density and kinematic viscosity as a function of temperature (T) and salinity (S) (Table 2): (1) giant ooids composed of aragonite under conditions similar to modern carbonate platforms ($T = 25^\circ\text{C}$); (2) giant ooids composed of calcite under the same conditions as (1); (3) giant ooids composed of aragonite under warmer climate ($T = 40^\circ\text{C}$); and (4) giant ooids composed of ikaite ($T = 0^\circ\text{C}$). Ikaite is a hydrated calcium carbonate mineral ($\text{CaCO}_3 \cdot 6\text{H}_2\text{O}$) that precipitates only at cold temperatures ($< 4^\circ\text{C}$) and rapidly dehydrates to monohydrated calcite, calcite, aragonite, or vaterite at warmer temperatures (timescales of hours to days) (Bischoff et al., 1993a; Ito, 1998; Shaikh, 1990; Tang et al., 2009) or after any subaerial exposure (Smoot & Lowenstein, 1991). In theory, due to the rapid and early transformation of ikaite to aragonite (or other CaCO_3 phases), fabrics interpreted as having been originally composed of aragonite may not be inconsistent with ikaite as a precursor. The latter scenarios were predicted to be more amenable to larger equilibrium ooid sizes, either due to higher precipitation rate at a warmer temperature or due to lower abrasion rate resulting from the low density of ikaite and high viscosity of cold seawater. Kinetic parameters for aragonite and calcite precipitation at 25°C , aragonite at 40°C , and ikaite at 0°C were chosen from Zhong and Mucci (1989), Burton and Walter (1987), and Papadimitriou et al. (2014), respectively (Table 2). Results for aragonite and calcite at $T = 0^\circ\text{C}$ were not included in the following analysis because their sluggish precipitation kinetics at low temperature (Burton & Walter, 1987; Lopez et al., 2009) make them an implausible alternative to ikaite (Figure S5).

PHREEQC (Parkhurst & Appelo, 2013) was used to estimate combinations of $p\text{CO}_2$ and ALK required for the Ω values determined for each of the four scenarios (Supplementary Text S1). A range of alkalinity from 2 to 10 meq/L and a range of $p\text{CO}_2$ from $10^{-2.5}$ to 10^{-5} atm (consistent with constraints from Kasting, 1987; Kasting, 1993; and Sheldon, 2006) were explored. The PHREEQC database (Parkhurst & Appelo, 2013) was applied for aragonite/calcite at $T = 25^\circ\text{C}$, 40°C and the FREZCHEM database (Marion et al., 2010) was applied for ikaite at $T = 0^\circ\text{C}$. The concentration of Ca^{2+} was constrained as a function of alkalinity, with either $\text{Ca:ALK} = 5$ (i.e., modern seawater) or $\text{Ca:ALK} = 0.75$, the minimum estimate from Blättler et al. (2016); and the concentration of Mg^{2+} was constrained as a function of $[\text{Ca}^{2+}]$, with either $\text{Mg:Ca} = 1$ or $\text{Mg:Ca} = 5$, following endmember values from Hardie (2003).

3 Results

The carbonate mineral saturation states required for giant ooids with $D = 10$ mm varied substantially depending on mineralogy (aragonite, calcite, or ikaite) and temperature ($T = 0^\circ\text{C}$, 25°C , 40°C) (Figure 1). Aragonitic or calcitic ooids of this size under conditions similar to those on modern carbonate platforms (i.e., $T = 25^\circ\text{C}$) required $\Omega_{\text{aragonite}} \cong 19$ or $\Omega_{\text{calcite}} \cong 26$ (Figure 1a-b), both of which are notably higher than saturation states observed in modern shallow marine settings (e.g., $\Omega_{\text{aragonite}} = 5$ in the Turks and Caicos Islands, Trower et al., 2018). In contrast, aragonitic giant ooids at $T = 40^\circ\text{C}$ required $\Omega_{\text{aragonite}} \cong 10$ (Figure 1c) and ikaite giant ooids at $T = 0^\circ\text{C}$ required $\Omega_{\text{ikaite}} \cong 4$ (Figure 1d). Smaller giant ooids ($D = 5$ mm) required lower saturation states— $\Omega_{\text{aragonite}} \cong 12$ or $\Omega_{\text{calcite}} \cong 17$ for $T = 25^\circ\text{C}$, $\Omega_{\text{aragonite}} \cong 7$ for $T = 40^\circ\text{C}$, or $\Omega_{\text{ikaite}} \cong 2$ for $T = 0^\circ\text{C}$. PHREEQC results illustrated that all cases required $\text{ALK} > 2$ meq/L and $p\text{CO}_2 \leq 10^{-2.5}$ atm ($\sim 10\times$ present atmospheric level, PAL) (Figure 2); the lowest minimum ALK values were associated with $\text{Ca:ALK} = 5$, which is most consistent with a minimum constraint of $[\text{Ca}] \geq 9\text{mM}$ from late Tonian fluid inclusion data (Spear et al., 2014) and constraints from Ca isotopes (Blättler et al., 2020). The $\text{Mg:Ca} = 5$ cases required higher alkalinity and lower $p\text{CO}_2$ than $\text{Mg:Ca} = 1$ cases; $\text{Mg:Ca} = 5$ is most consistent with Hardie's (2003) estimates of Cryogenian and Ediacaran seawater. The ikaite scenario required somewhat higher ALK and lower $p\text{CO}_2$ than the other scenarios because ikaite is more soluble than aragonite or calcite. In all cases, most of the combinations of $p\text{CO}_2$ and alkalinity that were consistent with giant ooid formation occurred at $\text{pH} \geq 8.2$ (Kasemann et al., 2010), although cases with $\text{Ca:ALK} = 5$ allowed giant

ooid formation at $\text{pH} \leq 8.2$ at elevated pCO_2 (Figure 2). The model results suggested that giant ooid formation is not consistent with $\text{pH} = 7\text{--}7.2$ (Isson and Planavsky, 2018) (Figure 2).

The constraints on $\Omega_{\text{aragonite}}$ and Ω_{calcite} were relatively insensitive to the choice of u_* and therefore transport mode, suggesting that the requirements for $\Omega_{\text{aragonite}}$ and Ω_{calcite} are consistent even for pill-shaped giant ooids (Singh 1987; Hood and Wallace, 2018) associated with transport via rolling and sliding rather than saltation (Sipos et al., 2018). The constraint on Ω_{ikaite} was somewhat more sensitive to the choice of u_* , such that transport via rolling and sliding required higher Ω_{ikaite} than transport via saltation.

4 Discussion

The combinations of elevated ALK and relatively low pCO_2 indicated in all scenarios (Figure 2) could be consistent with drawdown of CO_2 and increased seawater alkalinity due to enhanced weathering prior to the Snowball glaciations (Cox et al., 2016; Donnadieu et al., 2004; Godd  ris et al., 2003; Hoffman et al., 1998), while Ediacaran giant ooid occurrences suggest that elevated alkalinity also characterized Ediacaran seawater. However, not all scenarios are equally plausible. The set of carbonate chemistry models with $\text{Ca:ALK} = 5$ and $\text{Mg:Ca} = 5$ are most consistent with constraints from fluid inclusion data (Spear et al., 2014), Ca isotopes (Bl  ttler et al., 2020), and mid-ocean ridge flux modeling (Hardie, 2003) (Figure 2). Although Neoproterozoic carbonate successions have been interpreted to have formed under conditions similar to modern tropical carbonate platforms (e.g., Hoffman et al., 1998), the high Ω values implied by the 25°C scenarios are not particularly plausible solutions. It is unlikely that the Ω values required for $D = 10$ mm ($\Omega_{\text{aragonite}} \cong 19$ or $\Omega_{\text{calcite}} \cong 26$) could be sustained over the >1000 year timescales necessary for ooid growth (Beaupr   et al., 2015; Duguid et al., 2010). Both Ω values are above the thresholds for homogeneous nucleation of aragonite or calcite, respectively (Morse & He, 1993; Pokrovsky, 1998; Sun et al., 2015); at these Ω values, the respective carbonate mineral would have nucleated rapidly both on available surfaces (heterogeneous nucleation)—including ooid surfaces, particulate organic matter, etc.—and spontaneously within the water column (homogeneous nucleation). Furthermore, the rapid CaCO_3 nucleation/precipitation at high Ω values and the relatively slow rate of CO_2 hydration/hydroxylation (Zeebe & Wolf-Gladrow, 2001) would both provide strong negative

feedbacks on Ω . Although the $T = 25^\circ\text{C}$ $\Omega_{\text{aragonite}}$ or Ω_{calcite} values for $D = 5$ mm are more plausible from this perspective, they are not consistent with the observations of ooids with $D > 5$ mm. Based on the common occurrence of giant ooids with diameters ≥ 10 mm, it is therefore more likely that Neoproterozoic giant ooids formed under conditions that were either much warmer ($T = 40^\circ\text{C}$) or much colder ($T = 0^\circ\text{C}$) than modern carbonate platforms.

The warmer scenario can explain aragonitic giant ooids under a range of bed shear velocities, but only with infrequent sediment transport (Figure 1, Figure S4). Temperatures $\geq 40^\circ\text{C}$ at low latitudes are consistent with models of post-Snowball greenhouse climate (Le Hir et al., 2009; Pierrehumbert et al., 2011; Yang et al., 2017), although these models require $\text{pCO}_2 \cong 400\times \text{PAL}$ ($\sim 10^{-0.9}$ atm), implying exceptionally high ALK (>40 meq/L). Due to the reduced solar luminosity during Neoproterozoic time relative to the present (Gough, 1981), models with $\text{pCO}_2 \cong 10^{-2.7}$ atm have predicted a cooler-than-modern climate (i.e., inconsistent with $T = 40^\circ\text{C}$), and that $\text{pCO}_2 \lesssim \text{PAL}$ was sufficiently low to trigger global glaciation (Donnadieu et al., 2004; Hyde et al., 2000; Micheels & Montenari, 2008; Pierrehumbert et al., 2011). This scenario therefore requires that $\text{pCO}_2 > 10^{-2.7}$ atm—and, consequently, $\text{ALK} > 5$ meq/L—but also that $\text{pCO}_2 \ll 10^{-0.9}$ atm, such that Ω could be sufficiently elevated. The occurrences of giant ooids that stratigraphically underlie Marinoan glacial deposits could therefore be indicative of the persistence of greenhouse conditions after the Sturtian Snowball Earth (Mills et al., 2011), but would still have required some drawdown of CO_2 (Figure 2). This scenario would also imply hot low-latitude climate preceding the Sturtian Snowball Earth. Finally, for Ediacaran giant ooid occurrences, this scenario could be consistent with elevated carbonate clumped isotope temperatures from the Ediacaran Nafun Group (Bergmann et al., 2018), but is warmer than 20–25°C temperature estimates from fluid inclusions in Ediacaran halites deposited at equatorial latitudes (Meng et al., 2011).

Although the cold scenario requires higher ALK (6–10 meq/L) and lower pCO_2 ($\sim 10^{-4}$) than other cases, it is potentially consistent with several lines of evidence from the rock record. Glendonite—a pseudomorph of ikaite—has been reported in Cryogenian (James et al., 2005) and Ediacaran (Wang et al., 2017) carbonate units deposited prior to glaciogenic sediments. In the former case, glendonites are described in close stratigraphic association with giant ooids; model results demonstrate that aragonitic giant ooids cannot form at the cold temperatures at which

ikaite precipitates due to sluggish precipitation kinetics (Figure S5). Ooids formed in cold-water conditions have also been observed adjacent to glaciers in Antarctica (Goodwin et al., 2018; Rao et al., 1998) and in Cryogenian carbonates interpreted as glaciolacustrine deposits (Fairchild et al., 2016), although neither case has been definitively identified as having initially precipitated as ikaite. Furthermore, there is reason to suspect that ikaite might be substantially under-recognized in the rock record due to its rapid transformation to calcite and aragonite at temperatures only modestly above 0°C or after subaerial exposure. Analysis of modern and Holocene carbonates in lakes in California and Patagonia has suggested that most of this carbonate originally precipitated as ikaite before transforming to calcite or aragonite during warmer seasons (Bischoff, et al., 1993b; Council & Bennett, 1993; Oehlerich et al., 2013). In these cases, ikaite had not been recognized as the dominant primary phase until identified via analyses of modern samples because the crystal size of much of the primary ikaite was much smaller than the characteristic glendonite pseudomorphs. It is not yet clear how one might distinguish the petrographic fabrics of finely-crystalline primary aragonite vs. ikaite transformed to aragonite in the rock record. This scenario, if correct, implies that Cryogenian giant ooids are an indicator facies of cold conditions at low-latitudes prior to the delivery of glacially-derived sediment, with the consequence that strata associated with giant ooids could provide a record of ecosystem responses to this extreme cooling. Notably, formation of ooids of any size also requires current transport, so this scenario would also require areas of open water in order for waves to interact with the seafloor. This scenario is less plausible for Ediacaran giant ooid occurrences, given that two of the four occurrences likely postdate the Gaskiers glaciation (Table 1).

The results presented here illustrate that Neoproterozoic giant ooids must be reconciled with at least one surprising finding. The $T = 40^{\circ}\text{C}$ scenario requires a hot, high pCO_2 climate not long before the initiation of each Neoproterozoic glaciation and at moderate latitudes during Ediacaran time. These conditions could be consistent with the persistence of post-Snowball greenhouse climate and match the reported aragonitic mineralogy of many giant ooid occurrences (Hood and Wallace, 2018), but are potentially problematic for giant ooids that directly underlie glacially-deposited sediments or that occur in close stratigraphic association with glendonite (James et al., 2005). The $T = 0^{\circ}\text{C}$ scenario requires an original primary mineralogy that is currently considered geologically rare and suggests that low latitude seawater was already cold prior to the onset of glacially-derived sediment deposition. Both scenarios

require seawater alkalinity >5 meq/L and infrequent sediment transport. Conditions with more frequent sediment transport cannot produce giant ooids due to the rapid abrasion rates of large particles (Figures S3, S4). Ikaite giant ooids are theoretically possible at lower bed shear velocities and somewhat more frequent sediment transport than aragonite giant ooids (Figure 2, Figure S4). Detailed sedimentological analyses of giant-ooid bearing units (e.g., bedform dimensions, grain-boundary cements) could therefore enable more robust tests of these two scenarios, combined with improved age constraints and a framework for identifying the diagenetic products of finely-crystalline ikaite. The finding that giant ooid formation is most plausible at extreme temperatures—in addition to requiring high alkalinity, strong currents necessary to transport large particles, and infrequent sediment transport—may finally explain why they are so uncommon in the rock record.

Acknowledgments, Samples, and Data

The author thanks Carl Simpson and Miquela Ingalls for helpful discussions; the author also thanks reviewers Dawn Sumner and Ashleigh Hood for their insightful comments. Data supporting the conclusions are provided in the figures, table, supplementary information, and cited references. Matlab code used to calculate equilibrium ooid sizes is archived at: <https://doi.org/10.5281/zenodo.3601507>

References

- Attal, M., & Lavé, J. (2009). Pebble abrasion during fluvial transport: Experimental results and implications for the evolution of the sediment load along rivers. *Journal of Geophysical Research*, 114(F4), 607.
- Batten, K. L., Narbonne, G. M., & James, N. P. (2004). Paleoenvironments and growth of early Neoproterozoic calcimicrobial reefs: platformal Little Dal Group, northwestern Canada. *Precambrian Research*, 133(3), 249–269.
- Beaupré, S. R., Roberts, M. L., Burton, J. R., & Summons, R. E. (2015). Rapid, high-resolution ^{14}C chronology of ooids. *Geochimica et Cosmochimica Acta*, 159, 126–138.
- Bergmann, K. D., Zentmyer, R. A., & Fischer, W. W. (2011). The stratigraphic expression of a large negative carbon isotope excursion from the Ediacaran Johnnie Formation, Death Valley. *Precambrian Research*, 188(1), 45–56.

- Bergmann, K. D., Al Balushi, S. A. K., Mackey, T. J., Grotzinger, J. P., & Eiler, J. M. (2018). A 600-Million-Year Carbonate Clumped-Isotope Record from the Sultanate of Oman. *Journal of Sedimentary Research*, 88(8), 960–979.
- Bischoff, J. L., Fitzpatrick, J. A., & Rosenbauer, R. J. (1993a). The Solubility and Stabilization of ikaite ($\text{CaCO}_3 \cdot 6\text{H}_2\text{O}$) from 0° to 25°C: Environmental and Paleoclimatic: Implications for Thinalite Tufa. *The Journal of Geology*, 101, 21–33.
- Bischoff, J. L., Stine, S., Rosenbauer, R. J., Fitzpatrick, J. A., & Stafford, T. W. (1993b). Ikaite precipitation by mixing of shoreline springs and lake water, Mono Lake, California, USA. *Geochimica et Cosmochimica Acta*, 57(16), 3855–3865.
- Blättler, C. L., Kump, L. R., Fischer, W. W., Paris, G., Kasbohm, J. J., & Higgins, J. A. (2016). Constraints on ocean carbonate chemistry and pCO_2 in the Archaean and Palaeoproterozoic. *Nature Geoscience*, 10, 41.
- Blättler, C. L., Bergmann, K. D., Kah, L. C., Gómez-Pérez, I., & Higgins, J. A. (2020). Constraints on Meso- to Neoproterozoic seawater from ancient evaporite deposits. *Earth and Planetary Science Letters*, 532, 115951.
- Burton, E. A., & Walter, L. M. (1987). Relative precipitation rates of aragonite and Mg calcite from seawater: Temperature or carbonate ion control? *Geology*, 15, 111–114.
- Carling, P. A. (1999). Subaqueous gravel dunes. *Journal of Sedimentary Research*, 69(3), 534–545.
- Chumakov, N. M. (2007). Climates and climate zonality of the Vendian: geological evidence. *Geological Society, London, Special Publications*, 286(1), 15–26.
- Council, T. C., & Bennett, P. C. (1993). Geochemistry of ikaite formation at Mono Lake, California: Implications for the origin of tufa mounds. *Geology*, 21(11), 971–974.
- Cox, G. M., Halverson, G. P., Stevenson, R. K., Vokaty, M., Poirier, A., Kunzmann, M., et al. (2016). Continental flood basalt weathering as a trigger for Neoproterozoic Snowball Earth. *Earth and Planetary Science Letters*, 446, 89–99.

- Day, E. S., James, N. P., Narbonne, G. M., & Dalrymple, R. W. (2004). A sedimentary prelude to Marinoan glaciation, Cryogenian (Middle Neoproterozoic) Keele Formation, Mackenzie Mountains, northwestern Canada. *Precambrian Research*, 133(3), 223–247.
- Dietrich, W. E. (1982). Settling velocity of natural particles. *Water Resources Research*, 18(6), 1615–1626.
- Donnadieu, Y., Godd  ris, Y., Ramstein, G., N  d  lec, A., & Meert, J. (2004). A “snowball Earth” climate triggered by continental break-up through changes in runoff. *Nature*, 428(6980), 303–306.
- Duguid, S. M. A., Kyser, T. K., James, N. P., & Rankey, E. C. (2010). Microbes and Ooids. *Journal of Sedimentary Research*, 80(3), 236–251.
- Evans, D. A. D. (2000). Stratigraphic, geochronological, and paleomagnetic constraints upon the Neoproterozoic climatic paradox. *American Journal of Science*, 300(5), 347–433.
- Fairchild, I. J., Fleming, E. J., Bao, H., Benn, D. I., Boomer, I., Dublyansky, Y. V., et al. (2016). Continental carbonate facies of a Neoproterozoic panglaciation, north-east Svalbard. *Sedimentology*, 63(2), 443–497.
- Fromhold, T. A., & Wallace, M. W. (2011). Nature and significance of the Neoproterozoic Sturtian–Marinoan Boundary, Northern Adelaide Geosyncline, South Australia. *Australian Journal of Earth Sciences*, 58(6), 599–613.
- Godd  ris, Y., Donnadieu, Y., N  d  lec, A., Dupr  , B., Dessert, C., Grard, A., et al. (2003). The Sturtian “snowball” glaciation: fire and ice. *Earth and Planetary Science Letters*, 211(1), 1–12.
- Goodwin, I. D., Roberts, J. L., & Etheridge, D. M. (2018). Modern to Glacial age subglacial meltwater drainage at Law Dome, coastal East Antarctica from topography, sediments and j  kulhlaup observations. *Geological Society, London, Special Publications*, 461, 215–230.
- Gough, D. O. (1981). Solar Interior Structure and Luminosity Variations. In *Physics of Solar Variations* (pp. 21–34). Springer Netherlands.

- Grotzinger, J. P., & James, N. P. (2000). Precambrian carbonates: evolution of understanding. In J. P. Grotzinger & N. P. James (Eds.), *Carbonate Sedimentation and Diagenesis in the Evolving Precambrian World* (Vol. 67, pp. 3–20). SEPM Special Publication.
- Gutstadt, A. M. (1968). Petrology and depositional environments of the Beck Spring Dolomite (Precambrian), Kingston Range, California. *Journal of Sedimentary Petrology*, 38(4), 1280–1289.
- Hardie, L. A. (2003). Secular variations in Precambrian seawater chemistry and the timing of Precambrian aragonite seas and calcite seas. *Geology*, 31(9), 785–788.
- Hoffman, P. F., & Li, Z.-X. (2009). A palaeogeographic context for Neoproterozoic glaciation. *Palaeogeography, Palaeoclimatology, Palaeoecology*, 277(3), 158–172.
- Hoffman, P. F., Kaufman, A. J., Halverson, G. P., & Schrag, D. P. (1998). A neoproterozoic snowball earth. *Science*, 281(5381), 1342–1346.
- Hoffman, P. F., Abbot, D. S., Ashkenazy, Y., Benn, D. I., Brocks, J. J., Cohen, P. A., et al. (2017). Snowball Earth climate dynamics and Cryogenian geology-geobiology. *Science Advances*, 3(11), e1600983.
- Hood, A. van S., & Wallace, M. W. (2018). Neoproterozoic marine carbonates and their paleoceanographic significance. *Global and Planetary Change*, 160, 28–45.
- Hyde, W. T., Crowley, T. J., Baum, S. K., & Peltier, W. R. (2000). Neoproterozoic “snowball Earth” simulations with a coupled climate/ice-sheet model. *Nature*, 405(6785), 425–429.
- Isson, T. T., & Planavsky, N. J. (2018). Reverse weathering as a long-term stabilizer of marine pH and planetary climate. *Nature*, 560(7719), 471–475.
- Ito, T. (1998). Factors controlling the transformation of natural ikaite from Shiowakka, Japan. *Geochemical Journal*, 32, 267–273.
- James, N. P., Narbonne, G. M., Dalrymple, R. W., & Kurtis Kyser, T. (2005). Glendonites in Neoproterozoic low-latitude, interglacial, sedimentary rocks, northwest Canada: Insights into the Cryogenian ocean and Precambrian cold-water carbonates. *Geology*, 33(1), 9–12.

- Kasemann, S. A., Prave, A. R., Fallick, A. E., Hawkesworth, C. J., & Hoffmann, K.-H. (2010). Neoproterozoic ice ages, boron isotopes, and ocean acidification: Implications for a snowball Earth. *Geology*, 38(9), 775–778.
- Kasting, J. F. (1987). Theoretical constraints on oxygen and carbon dioxide concentrations in the Precambrian atmosphere. *Precambrian Research*, 34, 205–229.
- Kasting, J. F. (1993). Earth’s early atmosphere. *Science*, 259(5097), 920–926.
- Kirschvink, J. L. (1992). Late Proterozoic Low-Latitude Global Glaciation: the Snowball Earth. In J. W. Schopf & C. Klein (Eds.), *The Proterozoic biosphere : a multidisciplinary study* (pp. 51–52). New York: Cambridge University Press.
- Lamb, M. P., Dietrich, W. E., & Sklar, L. S. (2008). A model for fluvial bedrock incision by impacting suspended and bed load sediment. *Journal of Geophysical Research*, 113(F3), 225.
- Lapotre, M. G. A., Lamb, M. P., & McElroy, B. (2017). What sets the size of current ripples? *Geology*, 45(3), 243–246.
- Le Hir, G., Donnadieu, Y., Godd  ris, Y., Pierrehumbert, R. T., Halverson, G. P., Macouin, M., et al. (2009). The snowball Earth aftermath: Exploring the limits of continental weathering processes. *Earth and Planetary Science Letters*, 277(3), 453–463.
- Lopez, O., Zuddas, P., & Faivre, D. (2009). The influence of temperature and seawater composition on calcite crystal growth mechanisms and kinetics: Implications for Mg incorporation in calcite lattice. *Geochimica et Cosmochimica Acta*, 73(2), 337–347.
- Macdonald, F. A., Jones, D. S., & Schrag, D. P. (2009a). Stratigraphic and tectonic implications of a newly discovered glacial diamictite–cap carbonate couplet in southwestern Mongolia. *Geology*, 37(2), 123–126.
- Macdonald, F. A., McClelland, W. C., Schrag, D. P., & Macdonald, W. P. (2009b). Neoproterozoic glaciation on a carbonate platform margin in Arctic Alaska and the origin of the North Slope subterrane. *GSA Bulletin*, 121(3-4), 448–473.
- Marion, G. M., Mironenko, M. V., & Roberts, M. W. (2010). FREZCHEM: A geochemical model for cold aqueous solutions. *Computers & Geosciences*, 36(1), 10–15.

- Meng, F., Ni, P., Schiffbauer, J. D., Yuan, X., Zhou, C., Wang, Y., & Xia, M. (2011). Ediacaran seawater temperature: Evidence from inclusions of Sinian halite. *Precambrian Research*, 184(1), 63–69.
- Micheels, A., & Montenari, M. (2008). A snowball Earth versus a slushball Earth: Results from Neoproterozoic climate modeling sensitivity experiments. *Geosphere*, 4(2), 401–410.
- Mills, B., Watson, A. J., Goldblatt, C., Boyle, R., & Lenton, T. M. (2011). Timing of Neoproterozoic glaciations linked to transport-limited global weathering. *Nature Geoscience*, 4(12), 861–864.
- Morse, J. W., & He, S. (1993). Influences of T, S and PCO₂ on the pseudo-homogeneous precipitation of CaCO₃ from seawater: implications for whiting formation. *Marine Chemistry*, 41(4), 291–297.
- Nayar, K. G., Sharqawy, M. H., Banchik, L. D., & Lienhard, J. H., V. (2016). Thermophysical properties of seawater: A review and new correlations that include pressure dependence. *Desalination*, 390, 1–24.
- Oehlerich, M., Mayr, C., Griesshaber, E., Lücke, A., Oeckler, O. M., Ohlendorf, C., et al. (2013). Ikaite precipitation in a lacustrine environment – implications for palaeoclimatic studies using carbonates from Laguna Potrok Aike (Patagonia, Argentina). *Quaternary Science Reviews*, 71, 46–53.
- Papadimitriou, S., Kennedy, H., Kennedy, P., & Thomas, D. N. (2014). Kinetics of ikaite precipitation and dissolution in seawater-derived brines at sub-zero temperatures to 265K. *Geochimica et Cosmochimica Acta*, 140, 199–211.
- Parkhurst, D. L., & Appelo, C. A. J. (2013). Description of Input and Examples for PHREEQC Version 3—A Computer Program for Speciation, Batch-Reaction, One-Dimensional Transport, and Inverse Geochemical Calculations (No. Techniques and Methods 6–A43). USGS.
- Pelechaty, S. M. (1998). Integrated chronostratigraphy of the Vendian System of Siberia: implications for a global stratigraphy. *Journal of the Geological Society*, 155(6), 957–973.

- Petrov, P. Y. (2018). Postglacial Deposits of the Dal'nyaya Taiga Group: Early Vendian in the Ura Uplift, Siberia. Communication 2. Ura and Kalancha Formations and History of the Basin. *Lithology and Mineral Resources*, 53(6), 473–488.
- Pierrehumbert, R. T., Abbot, D. S., Voigt, A., & Koll, D. (2011). Climate of the Neoproterozoic. *Annual Review of Earth and Planetary Sciences*, 39(1), 417–460.
- Pokrovsky, O. S. (1998). Precipitation of calcium and magnesium carbonates from homogeneous supersaturated solutions. *Journal of Crystal Growth*, 186(1), 233–239.
- Rao, C. P., Goodwin, I. D., & Gibson, J. A. E. (1998). Shelf, coastal and subglacial polar carbonates, East Antarctica. *Carbonates and Evaporites*, 13(2), 174–188.
- Shaikh, A. M. (1990). A new crystal growth form of vaterite, CaCO₃. *Journal of Applied Crystallography*, 23, 263–265.
- Sharqawy, M. H., Lienhard, J. H., & Zubair, S. M. (2010). Thermophysical properties of seawater: a review of existing correlations and data. *Desalination and Water Treatment*, 16(1-3), 354–380.
- Sheldon, N. D. (2006). Precambrian paleosols and atmospheric CO₂ levels. *Precambrian Research*, 147(1), 148–155.
- Singh, U. (1987). Ooids and cements from the late Precambrian of the Flinders Ranges, South Australia. *Journal of Sedimentary Petrology*, 57(1), 117–127.
- Sipos, A. A., Domokos, G., & Jerolmack, D. J. (2018). Shape evolution of ooids: a geometric model. *Scientific Reports*, 8(1), 1758.
- Sklar, L. S., & Dietrich, W. E. (2004). A mechanistic model for river incision into bedrock by saltating bed load. *Water Resources Research*, 40(6).
- Smith, E.F., MacDonald, F.A., Crowley, J.L., Hodgins, E.B., and Schrag, D.P. (2016). Tectonostratigraphic evolution of the c. 780–730 Ma Beck Spring Dolomite: Basin Formation in the core of Rodinia: *Geological Society, London, Special Publications*, 424, 213–239.

- 466 Smoot, J. P., & Lowenstein, T. K. (1991). Depositional Environments of Non-Marine
467 Evaporites. In J. L. Melvin (Ed.), *Evaporites, Petroleum and Mineral Resources* (Vol. 50,
468 pp. 189–348). Amsterdam: Elsevier.
- 469 Southard, J. B., & Boguchwal, L. A. (1990). Bed configuration in steady unidirectional water
470 flows; Part 2, Synthesis of flume data. *Journal of Sedimentary Research*, 60(5), 658–679.
- 471 Spear, N., Holland, H. D., Garcia-Veigas, J., Lowenstein, T. K., Giegengack, R., & Peters, H.
472 (2014). Analyses of fluid inclusions in Neoproterozoic marine halite provide oldest
473 measurement of seawater chemistry. *Geology*, 42(2), 103–106.
- 474 Srivastava, P. (2006). Meso–Neoproterozoic coated grains and palaeoecology of associated
475 microfossils: The Deoban Limestone, Lesser Himalaya, India. *Palaeogeography*,
476 *Palaeoclimatology, Palaeoecology*, 239(3), 241–252.
- 477 Sumner, D. Y., & Grotzinger, J. P. (1993). Numerical modeling of ooid size and the problem of
478 Neoproterozoic giant ooids. *Journal of Sedimentary Petrology*, 63(5), 974–982.
- 479 Sun, W., Jayaraman, S., Chen, W., Persson, K. A., & Ceder, G. (2015). Nucleation of metastable
480 aragonite CaCO₃ in seawater. *Proceedings of the National Academy of Sciences of the*
481 *United States of America*, 112(11), 3199–3204.
- 482 Swett, K., & Knoll, A. H. (1989). Marine pisolites from Upper Proterozoic carbonates of East
483 Greenland and Spitsbergen. *Sedimentology*, 36, 75–93.
- 484 Tang, C. C., Thompson, S. P., Parker, J. E., Lennie, A. R., Azough, F., & Kato, K. (2009). The
485 ikaite-to-vaterite transformation: new evidence from diffraction and imaging. *Journal of*
486 *Applied Crystallography*, 42(2), 225–233.
- 487 Teitz, M., & Mountjoy, E. W. (1989). The late Proterozoic Yellowhead carbonate platform west
488 of Jasper, Alberta. In H. H. J. Geldsetzer, N. P. James, & G. E. Tebbun (Eds.), *Reefs,*
489 *Canada and Adjacent Area* (Vol. 13, pp. 129–134). Canadian Society of Petroleum
490 Geologists.
- 491 Thorie, A., Mukhopadhyay, A., Banerjee, T., & Mazumdar, P. (2018). Giant ooids in a
492 Neoproterozoic carbonate shelf, Simla Group, Lesser Himalaya, India: An analogue
493 related to Neoproterozoic glacial deposits. *Marine and Petroleum Geology*, 98, 582–606.

- Trindade, R. I. F., & Macouin, M. (2007). Palaeolatitude of glacial deposits and palaeogeography of Neoproterozoic ice ages. *Comptes Rendus: Geoscience*, 339(3), 200–211.
- Trower, E. J., & Grotzinger, J. P. (2010). Sedimentology, diagenesis, and stratigraphic occurrence of giant ooids in the Ediacaran Rainstorm Member, Johnnie Formation, Death Valley region, California. *Precambrian Research*, 180(1-2), 113–124.
- Trower, E. J., Lamb, M. P., & Fischer, W. W. (2017). Experimental evidence that ooid size reflects a dynamic equilibrium between rapid precipitation and abrasion rates. *Earth and Planetary Science Letters*, 468, 112–118.
- Trower, E. J., Cantine, M. D., Gomes, M. L., Grotzinger, J. P., Knoll, A. H., Lamb, M. P., et al. (2018). Active Ooid Growth Driven By Sediment Transport in a High-Energy Shoal, Little Ambergris Cay, Turks and Caicos Islands. *Journal of Sedimentary Research*, 88(9), 1132–1151.
- Trower, E. J., Lamb, M. P., & Fischer, W. W. (2019). The origin of carbonate mud. *Geophysical Research Letters*, 46(5), 2696–2703.
- Wang, Z., Wang, J., Suess, E., Wang, G., Chen, C., & Xiao, S. (2017). Silicified glendonites in the Ediacaran Doushantuo Formation (South China) and their potential paleoclimatic implications. *Geology*, 45(2), 115–118.
- Yang, J., Jansen, M. F., Macdonald, F. A., & Abbot, D. S. (2017). Persistence of a freshwater surface ocean after a snowball Earth. *Geology*, 45(7), 615–618.
- Zeebe, R. E., & Wolf-Gladrow, D. (2001). CO₂ in Seawater: Equilibrium, Kinetics, Isotopes (Vol. 65). Amsterdam: Elsevier.
- Zenger, D. H. (1976). Dolomitization and dolomite “dikes” in the Wyman Formation (Precambrian), Northeastern Inyo Mountains, California. *Journal of Sedimentary Petrology*, 46(3), 457–462.
- Zhong, S., & Mucci, A. (1989). Calcite and aragonite precipitation from seawater solutions of various salinities: Precipitation rates and overgrowth compositions. *Chemical Geology*, 78(3-4), 283–299.

Figure Captions

Figure 1. Contour plots of equilibrium ooid size (mm) as a function of carbonate mineral saturation state (Ω) vs. bed shear velocity (u_*) for four scenarios: (a) aragonite giant ooids at $T = 25^\circ\text{C}$, (b) calcite giant ooids at $T = 25^\circ\text{C}$, (c) aragonite giant ooids at $T = 40^\circ\text{C}$, and (d) ikaite at 0°C . Solid bold lines indicate combinations of Ω and u_* consistent with $D_{eq} = 10$ mm; dashed bold lines indicate combinations of Ω and u_* consistent with $D_{eq} = 5$ mm. The range in u_* in each plot is consistent with $P = 2.5$ for grain sizes ranging from 1-10 mm (Figure S1). Notably, D_{eq} is more sensitive to Ω than u_* in all cases, so an exact constraint on u_* is not necessary to estimate Ω .

Figure 2. Contour plots of Ω as a function of $\log_{10}(\text{pCO}_2)$ vs. ALK for each of the four scenarios with Ca:ALK = 0.75 or 5 and Mg:Ca = 1 or 5. The solid bold black lines indicate the Ω value necessary for $D_{eq} = 10$ mm and the dashed bold black lines indicate the Ω value necessary for $D_{eq} = 5$ mm. The white lines indicate contours of pH = 7.5 (dotted line), pH = 8.2 (solid line), pH = 9 (dashed line), and pH = 9.5 (dash-dot line). pH = 8.2 is used as a benchmark following boron isotope constraints from Kasemann et al. (2010). Grey boxes illustrate most plausible conditions, as discussed in main text.

Table 1. Neoproterozoic giant ooid-bearing strata and their relationship with glacial deposits.

Giant-ooid-bearing unit	Grain diameters (mm) ^a	Overlying glacial unit and stratigraphic relationship	Paleolatitude range ^b	Reference(s)
Backlundtoppen Formation (Svalbard)	4-9 (maximum 14)	Elbobreen Formation, Petrovbrean Member (Sturtian), separated by ~300 m of carbonate-dominated stratigraphy	S 15-30°	Swett and Knoll (1989)
Beck Spring Dolomite (California, USA)	≤ 10	Kingston Peak Formation, Surprise Diamictite equivalent (Sturtian), separated by unit KP1 (fine-grained siliciclastic rocks interpreted as non-glacial based on	N 0-15°	Gutstadt (1968)

		lack of dropstones; 0-200 m thick—see Smith et al., 2016)		
Grainstone Formation, Little Dal Group (NW Canada)	2-10	Rapitan Group (Sturtian), separated by up to ~500 m of carbonate-dominated stratigraphy	N 0-15°	Batten et al. (2004)
Deoban Limestone (Lesser Himalaya, India)	≤ 6°	Blaini Group (Marinoan), not directly overlying	N 0-15°	Srivastava (2006)
Katakturuk Dolomite unit K1 (Alaska, USA)	> 4	Nularvik Cap Carbonate (Marinoan), directly overlying	S 0-15°	Macdonald, et al. (2009b)
Keele Formation (NW Canada)	≤ 5°	Ice Brook diamictite (Marinoan), separated by > 100m of siliclastic rocks of the upper Keele Formation	S 0-15°	Day et al. (2004)
Kunihar Formation, Simla Group (Lesser Himalaya, India)	2-24°	Blaini Group (Marinoan), separated by ~1 km thick Sanjauli and Chhaosa Formations, fluvial siliciclastic rocks	N 0-15°	Thorie et al. (2018)
Tayshir Member, Tsagaan Oloom Formation (Mongolia)	> 5°	Khongoryn diamictite (Marinoan), directly overlying	N 0-15°	Macdonald, et al. (2009a)
Trezona Formation (Australia)	≤ 16	Elatina Formation (Marinoan), separated by an unconformity and, locally, siliciclastic rocks of the Yaltipena Formation	N 0-15°	Singh (1987)
Yankaninna Formation and Weetootla Dolomite (Australia)	≤ 10°	Elatina Formation (Marinoan), separated by ~100-200 m of the shale-dominated Amberoona Formation and Enorama Shale	N 0-15°	Fromhold and Wallace (2011)
Byng Formation, Upper Miete Group (Alberta, Canada)	≤ 4.5	Unconformably overlain by Cambrian McNaughton Formation (no clear stratigraphic relationship with Ediacaran	S 30-45°	Teitz and Mountjoy (1989)

Gaskiers glaciation)

Johnnie Formation, Rainstorm Member (California, USA)	3.5 (maximum 12) ^c	Postdates Shuram C isotope excursion and Ediacaran Gaskiers glaciation (cf. Bergmann et al., 2011)	S 30-45°	Trower and Grotzinger (2010)
Kalancha Formation (Patom Basin, Siberia)	≤ 25	Zherba Formation (possibly correlated with Ediacaran Gaskiers glaciation based on C isotope work by Pelechaty, 1998)	S 15-30°	Petrov (2018)
Upper Wyman Formation and basal Reed Dolomite (California, USA)	≤ 5	Contemporaneous with Rainstorm Member?	S 30-45°	Zenger (1976)

^aGrain size data from Sumner and Grotzinger (1993) except where otherwise noted. Some examples listed in a recent compilation of giant ooid deposits by Thorie et al. (2018) with grain sizes not substantially > 2 mm are not included because those are not giant ooids, by definition, and their relatively small grain sizes are not useful for differentiating between different scenarios (Figure 1).

^bPaleolatitudes from compilation by Hoffman and Li (2009).

^cGrain size data from reference listed in “Reference(s)” column.

Table 2. Parameters for different model scenarios.

Fluid and mineral properties				Kinetic parameters			Source
	Salinity, S (ppt)	Sediment density, ρ_s (kg/m ³)	Fluid density, ρ_f (kg/m ³) ^a	Fluid kinematic viscosity, ν_f (m ² /s) ^a	k (μmol/m ² /hr)	n	
Scenario 1: aragonite, 25°C	35	2800	1025	9.37×10^{-7}	12.88	2.26	Zhong and Mucci (1989)
Scenario 2: calcite, 25°C	35	2700	1025	9.37×10^{-7}	0.783	2.87	Zhong and Mucci (1989)
Scenario 3: aragonite, 40°C	35	2800	1018	6.95×10^{-7}	45.1	2.4	Burton and Walter (1987)
Scenario 4:	50	1800	1040	1.89×10^{-6}	117.5	1.23	Papadimitriou

ikaite, 0°C

et al. (2014)

550 ^aSeawater density and kinematic viscosity determined following Nayar et al., 2016 and Sharqawy et al.,
551 2010.

Figure 1.

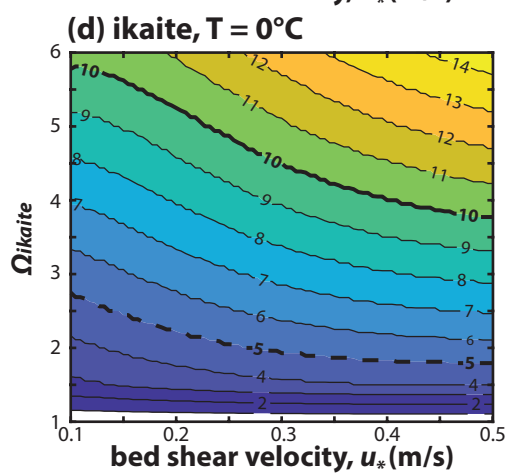
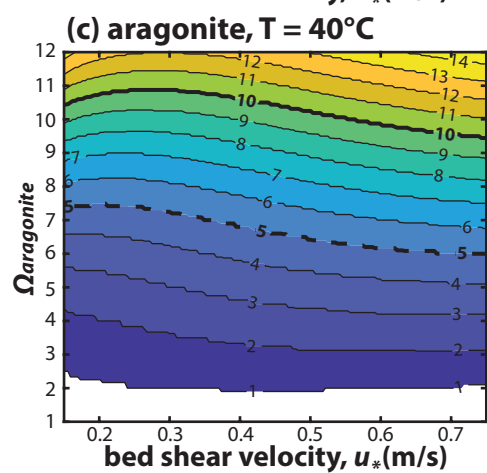
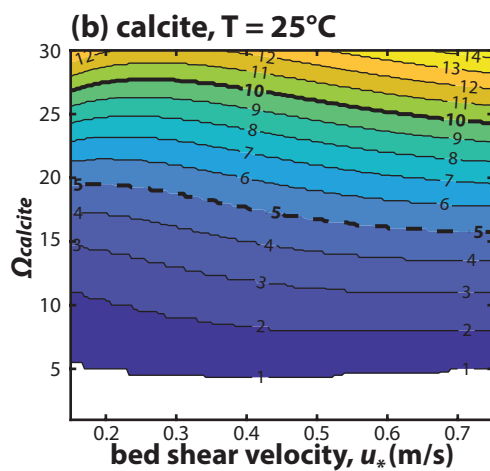
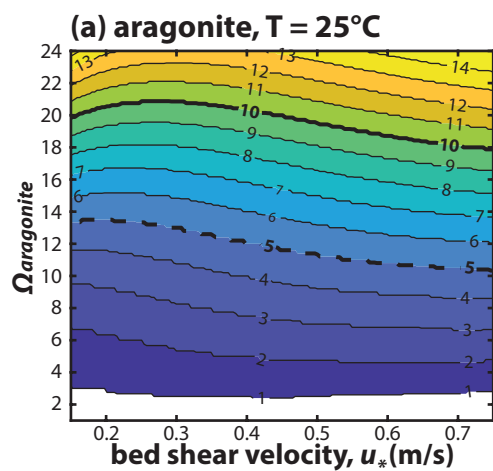


Figure 2.

